

Evaluation of Green's Function Integrals in Conducting Media

Swagato Chakraborty, *Student Member, IEEE*, and Vikram Jandhyala, *Senior Member, IEEE*

Abstract—This paper presents an accurate integration method for computing Green's function operators related to lossy conducting media. The presented approach is ultrawideband, i.e., the integration schemes cover the entire range of frequency behavior, from high frequencies where skin current is prevalent to low frequencies where volume current flow dominates. The scheme is a step toward permitting exact ultrawide-band frequency domain surface-only-based integral-equation simulation of arbitrarily-shaped three-dimensional conductors, and toward obviating the need for volume-based explicit frequency-dependent skin effect modeling. This work deals specifically with the computation of Green's functions and not with the unrelated but important low-frequency conditioning issue associated with the standard electric field integral equation.

Index Terms—Boundary element methods, conducting bodies, electromagnetic (EM) scattering, integral equations, skin effect.

I. INTRODUCTION

SURFACE and volumetric integral equation techniques are powerful paradigms for modeling electromagnetic (EM) interactions in integrated circuit (IC) and packaging problems. While coupled electromagnetic and circuit analyses have been successfully realized through the popular volumetric partial element equivalent circuit (PEEC) approach [1], [2] the search for more general approaches, especially for modeling frequency-dependent skin effects and for arbitrarily-shaped structures, has led to circuit-coupled surface-based electric field integral equation (EFIE) formulations [3], [4]. In these and other works [5]–[12] it has been shown that surface integral equations and method of moments (MoM) formulations can be interpreted and applied as generalizations of volumetric EFIE—based PEEC. At high frequencies, surface impedance approximations are sufficiently accurate to model losses and inductive behavior caused by skin effects. However, at lower frequencies, standard surface impedance approximations are invalid. Therefore, for broadband simulation as necessitated in digital or ultrawide-band systems, a volumetric formulation is typically required at low frequencies. However in a volumetric formulation, the skin effect needs to be modeled explicitly through a volume meshing. It is noted that some recent efforts

have been aimed at obtaining new surface impedance approximations [8].

Handling a mix of full-wave and skin-like effects with a surface-only formulation is desirable since frequency-dependent effects can be tracked without changing geometric discretization and without taking recourse to a special volume formulation at low frequencies. This is particularly true for small microelectronic structures where geometry detail and not wavelength is the guiding factor in mesh discretization. To accomplish a surface-only formulation valid for realistic conductors over a broad range of frequencies, the interior lossy medium EM problem must be addressed and coupled to the external medium model [10], and such a formulation requires explicit computation of the Green's function integrals in the interior lossy medium, in contrary to the volumetric formulation, where the Green's function integrals are always computed in the background medium.

This paper presents an exact formulation and accurate numerical quadrature scheme to efficiently compute highly damped Green's functions in lossy conductors. The presented method is general in terms of geometries, frequencies, material parameters, and relative separation and orientation of source and observer regions, and potentially forms an important step toward the realization of a surface-only ultrawide-band integral equation formulation.

It should be noted that the low frequency-dependence and modeling issue being addressed here is distinct from the classical low frequency ill-conditioning of an EFIE formulation. In fact, depending on the conductance involved, the issue discussed here can arise at much larger frequencies than those where the EFIE is inherently ill-conditioned. The treatment here is complementary to advances in improving EFIE conditioning [9] at low frequencies.

The presented quadrature scheme, discussing computation of the relevant Green's function integrals in lossy media using RWG functions in a PMCHW formulation, is initially facilitated by transforming the Green's function computation associated with RWG functions into polar coordinates. Subsequently, the proper order of integration results in one analytic integration along one coordinate. Finally, the remaining one-dimensional (1-D) integral is computed as a summation of several superposed integrals over different bands in the integration coordinate.

Section II of this paper presents the two-region formulation that utilizes the integrals that are the subject of this paper. Existing quadrature schemes are discussed in Section III. The specific frequency dependence of the integrals under study is outlined in Section IV. Section V presents the polar-coordinate-based integration schemes. Numerical results, self-consistency

Manuscript received October 28, 2002; revised October 29, 2003. This work was supported in part by the Defense Advanced Research Projects Agency-Microsystems Technology Office (DARPA-MTO) NeoCAD grant N66001-01-1-8920, the National Science Foundation (NSF) CAREER grant ECS-0093102, NSF-SRC Mixed-Signal Initiative grant CCR-0120371, and in part by a grant from Ansoft Corporation.

The authors are with the Department of Electrical Engineering, University of Washington, Seattle, WA 98195 USA (e-mail: jandhyala@ee.washington.edu; swagato@u.washington.edu).

Digital Object Identifier 10.1109/TAP.2004.836430

checks and comparisons with other techniques are detailed in Section VI, and Section VII presents conclusions and continuing work.

II. FORMULATION AND RESULTANT INTEGRALS

In a two-region surface equivalent problem [10], with the two regions being a homogeneous lossless background medium, typically free space or a lossless dielectric, and the interior of a realistic conductor, the exterior equivalent problem utilizes the background medium Green's function, while the lossy medium Green's function is required for the interior equivalent problem. For the EFIE, scalar and vector potential integrals will be necessitated, while for the magnetic field integral equation (MFIE), an integrand that represents the curl of the vector potential is required. In general, for PMCHW [10] and combined field integral equation (CFIE) formulations, all three types of integrands need to be computed.

Typically for a region characterized with material properties given by the permeability μ and permittivity ϵ , the electric and magnetic field \mathbf{E} and \mathbf{H} can be represented by the following:

$$\mathbf{E} = \mathbf{E}^{\text{inc}} - j\omega\mathbf{A} - \nabla\phi - \frac{1}{\epsilon}\nabla \times \mathbf{F} \quad (1a)$$

$$\mathbf{H} = \mathbf{H}^{\text{inc}} - j\omega\mathbf{F} - \nabla\psi + \frac{1}{\mu}\nabla \times \mathbf{A} \quad (1b)$$

where \mathbf{E}^{inc} and \mathbf{H}^{inc} are the incident electric and magnetic fields in the region, \mathbf{A} and \mathbf{F} are the magnetic and electric vector potentials, ϕ and ψ represent the electric and magnetic scalar potentials, $\omega = 2\pi f$ where f is the frequency of operation.

The scalar and vector potentials can be written in terms of the Green's function G and the electric and magnetic current density, \mathbf{J} and \mathbf{M} as follows:

$$\mathbf{A}(\mathbf{r}) = \frac{\mu}{4\pi} \int_{S'} G(\mathbf{r}, \mathbf{r}') \mathbf{J}(\mathbf{r}') ds' \quad (2a)$$

$$\mathbf{F}(\mathbf{r}) = \frac{\epsilon}{4\pi} \int_{S'} G(\mathbf{r}, \mathbf{r}') \mathbf{M}(\mathbf{r}') ds' \quad (2b)$$

$$\phi(\mathbf{r}) = \frac{j}{4\pi\epsilon\omega} \int_{S'} G(\mathbf{r}, \mathbf{r}') \nabla \cdot \mathbf{J}(\mathbf{r}') ds' \quad (2c)$$

$$\psi(\mathbf{r}) = \frac{j}{4\pi\mu\omega} \int_{S'} G(\mathbf{r}, \mathbf{r}') \nabla \cdot \mathbf{M}(\mathbf{r}') ds' \quad (2d)$$

where the Green's functions $G(\mathbf{r}, \mathbf{r}')$ for a source point \mathbf{r}' located in the source region S' , and an observation point \mathbf{r} is

$$G(\mathbf{r}, \mathbf{r}') = \frac{e^{-jk|\mathbf{r}-\mathbf{r}'|}}{|\mathbf{r}-\mathbf{r}'|} \quad (3)$$

where k is the wave number at an angular frequency ω for a material with σ , μ_r , ϵ_r as the conductivity, relative permeability and permittivity, respectively, and is given by

$$k = \omega \sqrt{\mu_0 \mu_r \epsilon_0 \left(\epsilon_r + \frac{\sigma}{j\omega\epsilon_0} \right)}. \quad (4)$$

Two auxiliary potentials $\mathbf{\Pi}$ and Γ , are introduced to represent the four potentials in (2) as, $\mathbf{A} = \mu\mathbf{\Pi}$, $\mathbf{F} = \epsilon\mathbf{\Gamma}$; $\phi = (\Gamma/\epsilon)$, $\psi = (\Gamma/\mu)$, where

$$\mathbf{\Pi}(\mathbf{r}) = \frac{1}{4\pi} \int_{S'} G(\mathbf{r}, \mathbf{r}') \mathbf{X}(\mathbf{r}') ds' \quad (5a)$$

$$\Gamma(\mathbf{r}) = \frac{j}{4\pi\omega} \int_{S'} G(\mathbf{r}, \mathbf{r}') \nabla \cdot \mathbf{X}(\mathbf{r}') ds'. \quad (5b)$$

Additionally, the curl operators in (1) are represented as

$$\nabla \times \mathbf{\Pi}(\mathbf{r}) = -\frac{1}{4\pi} \int_{S'} \nabla' G(\mathbf{r}, \mathbf{r}') \times \mathbf{X}(\mathbf{r}') ds' \quad (5c)$$

where \mathbf{X} represents the electric or magnetic current density. The popular triangle-pair-based Rao–Wilton–Glisson (RWG) functions [7] are used to represent $\mathbf{X}(\mathbf{r}')$, wherein current is modeled by edge-based piecewise linear vector functions, and the divergence of current is represented by piecewise constant scalar functions as $\mathbf{X}(\mathbf{r}) = (\boldsymbol{\rho}'^{\pm} l / 2A^{\pm})$, and $\nabla \cdot \mathbf{X}(\mathbf{r}) = (l/A^{\pm})$ [7] where $\boldsymbol{\rho}'^{\pm}$ represents the vector joining the node opposite to the edge in question to (from) the source point \mathbf{r}' in the positive (negative) triangle, A^{\pm} denotes the area of the positive (negative) triangle, and l is the length of the edge.

The generalized potential integrals (5) can be written for RWG sources as

$$\mathbf{\Pi}(\mathbf{r}) = \frac{l}{8\pi A} (\mathbf{M}_{\text{vect}} + \boldsymbol{\rho}^c M_{\text{scal}}) \quad (6a)$$

$$\Gamma(\mathbf{r}) = \frac{j l}{4\pi\omega A} M_{\text{scal}} \quad (6b)$$

$$\nabla \times \mathbf{\Pi}(\mathbf{r}) = \frac{l}{8\pi A} [\mathbf{R}^i \times (\mathbf{N}_{\text{vect}} + \boldsymbol{\rho}^c N_{\text{scal}})] \quad (6c)$$

where

$$\mathbf{M}_{\text{vect}} = \iint_T \boldsymbol{\rho} \frac{e^{-jkR}}{R} ds' \quad (7a)$$

$$M_{\text{scal}} = \iint_T \frac{e^{-jkR}}{R} ds' \quad (7b)$$

$$\mathbf{N}_{\text{vect}} = \iint_T \boldsymbol{\rho} \frac{e^{-jkR}(1+jkR)}{R^3} ds' \quad (7c)$$

$$N_{\text{scal}} = \iint_T \frac{e^{-jkR}(1+jkR)}{R^3} ds' \quad (7d)$$

and \mathbf{R}^i represents the vector joining the vertex of the source triangular region T (Fig. 1) opposite to the edge in question to the observation point, $\boldsymbol{\rho}^c$ is the vector from the same vertex to the projection of the observation point onto the plane of T , and $\boldsymbol{\rho}$ is the vector from the projection of the observation point \mathbf{r} on the plane of T to a source point \mathbf{r}' on T . $R = |\mathbf{r} - \mathbf{r}'|$, is the radial distance between the source and the observation point.

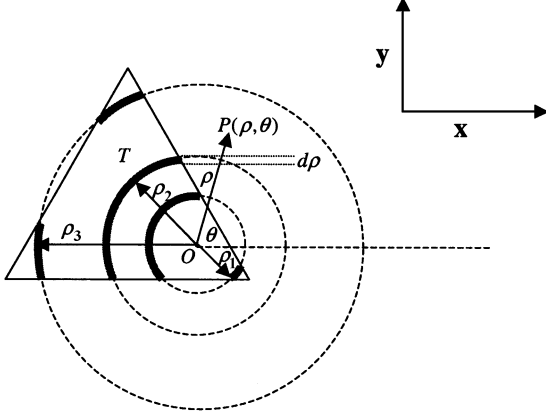


Fig. 1. Region of integration is shown for $(\rho = \rho_1, \rho_2, \rho_3)$, for a triangular region T , for the projection of the observation point on the plane of triangle o . Gray sections denote intervals of θ where the source point $P(\rho, \theta)$ lies within the triangle.

III. EXISTING ANALYTICAL AND NUMERICAL QUADRATURE SCHEME FOR EVALUATING GREEN'S FUNCTIONS

In the extant literature, evaluation of the potential integral (5) in free-space and low-loss media has been done by a variety of numerical schemes. For near-field terms, singularity extraction of the kernels in (5a) and (5b) is performed analytically [11], [12] to leave a function that can be integrated numerically with a low-order quadrature rule [13]. Recently, methods based on the Duffy transform have emerged, wherein the triangular integration region is transformed to a rectangle with a subsequent cancellation of the singularity. The integral in (5c) has been evaluated in free space [14], and in lossless dielectrics [10].

When the medium is conducting, even the singularity-extracted part may exhibit a rapid spatial decay, i.e., the extracted integral appears nearly singular when the observation point is sufficiently close to the source triangle. Hence, standard singularity extraction [11] fails to evaluate the integral accurately.

A suitable approach to Green's function computation in lossy media is polar coordinate integration, which can render the nonessential singularity cancelled through the Jacobian of transformation. Such methods are discussed previously in [15], [16] for lossless media and in [17] for lossy media, for the restricted case of the scalar Green's function in (7b). However, these methods are not sufficiently general for the integrals in (7a), (7c), and (7d) that are related to the vector potential or its curl. Another polar coordinate approach is proposed in [18] to evaluate the vector integral for the specific case of self-term integration. The method is extendable to the case when the observation point is located anywhere in the plane of the source triangle itself. This precludes the important case of observation at a near-singular point located above or below the source triangle, as occurs in thin conductors.

In Section V, we propose a general method for evaluating scalar, vector, and gradient Green's functions in lossy media with RWG basis functions. The presented technique works for all frequencies and for all relative positions between source triangles and observation points. The next section discusses the frequency-dependent behavior of the generalized potential integrals in conducting media that necessitates the specialized quadrature presented in later sections.

IV. FREQUENCY DEPENDENCE OF GREEN'S FUNCTIONS IN CONDUCTING MEDIA

The behavior of the Green's functions in (7) for conducting media is highly dependent on frequency. Consider a MoM [7] matrix created for interactions between RWG functions for the interior medium equivalent problem, which uses the conducting medium Green's functions. At high frequencies, the MoM matrix is nearly diagonal because of a very rapid exponential spatial decay of the conducting medium Green's function owing to the large imaginary part of the wave-number in (4).

At lower frequencies, the interactions between nonoverlapping RWG functions are not negligible; and the MoM matrix becomes progressively less sparse but has sections which are numerically sparse (e.g., in double precision arithmetic) due to large exponential decays. As the frequency is further lowered the MoM matrix is completely full while showing a weak exponential decay with distance. Eventually, the MoM matrix is full and the exponential decay is very weak or absent.

To summarize, at intermediate frequencies, between sharp fall-off and no fall-off regimes, special numerical treatment is required; the integrands presented by the lossy medium Green's function have sharp radial decay, and nonself interactions are also prominent. Depending on the frequency, the entire MoM matrix might be numerically significant. Fixed-order 2-D Gaussian quadrature rules in [13], that are popular in RWG-based MoM implementations will not provide accurate answers at such frequencies, owing to rapid decays of the Green's functions over finite distances.

V. COMPUTATION OF GENERALIZED POTENTIAL INTEGRALS IN CONDUCTING MEDIUM

The generalized potential integrals in (6) for RWG sources are constituted by the four terms in (7), which can be transformed into polar coordinates as follows:

$$\begin{aligned} \mathbf{M}_{\text{vect}} = & \hat{\mathbf{x}} \iint_T \frac{\rho^2 e^{-jk\sqrt{\rho^2+d^2}}}{\sqrt{\rho^2+d^2}} \cos \theta d\rho d\theta \\ & + \hat{\mathbf{y}} \iint_T \frac{\rho^2 e^{-jk\sqrt{\rho^2+d^2}}}{\sqrt{\rho^2+d^2}} \sin \theta d\rho d\theta \end{aligned} \quad (8a)$$

$$M_{\text{scal}} = \iint_T \frac{\rho e^{-jk\sqrt{\rho^2+d^2}}}{\sqrt{\rho^2+d^2}} d\rho d\theta \quad (8b)$$

$$\begin{aligned} \mathbf{N}_{\text{vect}} = & \hat{\mathbf{x}} \iint_T \frac{\rho^2 (1 + jk\sqrt{\rho^2+d^2}) e^{-jk\sqrt{\rho^2+d^2}}}{(\sqrt{\rho^2+d^2})^3} \\ & \times \cos \theta d\rho d\theta \\ & + \hat{\mathbf{y}} \iint_T \frac{\rho^2 (1 + jk\sqrt{\rho^2+d^2}) e^{-jk\sqrt{\rho^2+d^2}}}{(\sqrt{\rho^2+d^2})^3} \\ & \times \sin \theta d\rho d\theta \end{aligned} \quad (8c)$$

$$N_{\text{scal}} = \iint_T \frac{\rho (1 + jk\sqrt{\rho^2+d^2}) e^{-jk\sqrt{\rho^2+d^2}}}{(\sqrt{\rho^2+d^2})^3} d\rho d\theta. \quad (8d)$$

In the above equations, the $\hat{\mathbf{x}}$ and $\hat{\mathbf{y}}$ coordinates are local to the source triangle T (Fig. 1) and define the plane in which T lies. Also, d is the perpendicular distance of the observation point from the plane of T , and (ρ, θ) is the polar coordinate of a source point in T , with the projection of the observation point onto the plane of T as the origin. The scalar integrals in (8b) and (8d) and the scalar components of the vector integrals in (8a) and (8c) can be written in a generalized form, as

$$I_{\varphi\chi} = \int_{\rho} \int_{\theta} \varphi(\rho)\chi(\theta)d\rho d\theta \quad (9)$$

where φ is one of $\varphi_{M,\text{vect}}$, $\varphi_{M,\text{scal}}$, $\varphi_{N,\text{vect}}$, $\varphi_{N,\text{scal}}$ defined below as

$$\varphi_{M,\text{vect}}(\rho) = \frac{\rho^2 e^{-jk\sqrt{\rho^2+d^2}}}{\sqrt{\rho^2+d^2}} \quad (10a)$$

$$\varphi_{M,\text{scal}}(\rho) = \frac{\rho e^{-jk\sqrt{\rho^2+d^2}}}{\sqrt{\rho^2+d^2}} \quad (10b)$$

$$\varphi_{N,\text{vect}}(\rho) = \frac{\rho^2(1+jk\sqrt{\rho^2+d^2})e^{-jk\sqrt{\rho^2+d^2}}}{(\sqrt{\rho^2+d^2})^3} \quad (10c)$$

$$\varphi_{N,\text{scal}}(\rho) = \frac{\rho(1+jk\sqrt{\rho^2+d^2})e^{-jk\sqrt{\rho^2+d^2}}}{(\sqrt{\rho^2+d^2})^3}. \quad (10d)$$

Also, χ is one of χ_c , χ_s , χ_0 defined below as

$$\chi_c(\theta) = \cos \theta \quad (11a)$$

$$\chi_s(\theta) = \sin \theta \quad (11b)$$

$$\chi_0(\theta) = 1. \quad (11c)$$

Owing to the simple closed form expressions for the integral of $\chi(\theta)$, the integral $I_{\varphi\chi}$ can be recast as a function of ρ as

$$I_{\varphi\chi} = \iint_T \varphi(\rho)\chi(\theta)d\rho d\theta = \int_{\rho_{\min}}^{\rho_{\max}} \varphi(\rho)\xi(\rho)d\rho \quad (12)$$

where ρ_{\min} and ρ_{\max} are the extremal ρ for which $\exists \theta \ni P(\rho, \theta) \in T$, $P(\rho, \theta)$ denotes a point having coordinate (ρ, θ) (Fig. 1), and ξ is one of ξ_c , ξ_s , ξ_0 with

$$\begin{aligned} \begin{pmatrix} \xi_c(\rho) \\ \xi_s(\rho) \\ \xi_0(\rho) \end{pmatrix} &= \sum_{i=1}^{K(\rho)} \begin{pmatrix} \xi_c^i(\rho) \\ \xi_s^i(\rho) \\ \xi_0^i(\rho) \end{pmatrix} \\ &= \sum_{i=1}^{K(\rho)} \int_{\theta_{\min}^i(\rho)}^{\theta_{\max}^i(\rho)} \begin{pmatrix} \cos \theta \\ \sin \theta \\ 1 \end{pmatrix} d\theta \\ &= \sum_{i=1}^{K(\rho)} \begin{bmatrix} \sin \theta \\ -\cos \theta \\ \theta \end{bmatrix}_{\theta_{\min}^i(\rho)}^{\theta_{\max}^i(\rho)} \\ &= \sum_{i=1}^{K(\rho)} \begin{bmatrix} \sin \theta_{\max}^i(\rho) - \sin \theta_{\min}^i(\rho) \\ -\cos \theta_{\max}^i(\rho) + \cos \theta_{\min}^i(\rho) \\ \theta_{\max}^i(\rho) - \theta_{\min}^i(\rho) \end{bmatrix}. \quad (13) \end{aligned}$$

Also, $K(\rho)$ is the number of intervals (Fig. 1) in θ , $0 \leq \theta < 2\pi$, for which $P(\rho, \theta)$ lies in T , and θ_{\max}^i and θ_{\min}^i are the limits on θ for the i th interval. The values of $\theta_{\max}^i(\rho)$ and $\theta_{\min}^i(\rho)$ for each section are computed by obtaining the intersection of T and the circle of radius ρ centered at the projection of the observation point onto the plane of T . If the circle with radius ρ lies entirely in T , $K(\rho) = 1$, $\theta_{\max}^1 = 2\pi$, and $\theta_{\min}^1 = 0$. Hence

$$\begin{pmatrix} \xi_c(\rho) \\ \xi_s(\rho) \\ \xi_0(\rho) \end{pmatrix} = \begin{pmatrix} 0 \\ 0 \\ 2\pi \end{pmatrix}. \quad (14)$$

Alternatively, if for a given ρ , if the circle is completely outside T then the integral contributions are all zero. Consequently, the constituents of the generalized potential integrals (8) can be computed using (10)–(13) as

$$\begin{aligned} \mathbf{M}_{\text{vect}} &= \hat{\mathbf{x}} \int_{\rho_{\min}}^{\rho_{\max}} \varphi_{M,\text{vect}}(\rho)\xi_c(\rho)d\rho \\ &\quad + \hat{\mathbf{y}} \int_{\rho_{\min}}^{\rho_{\max}} \varphi_{M,\text{vect}}(\rho)\xi_s(\rho)d\rho \quad (15a) \end{aligned}$$

$$M_{\text{scal}} = \int_{\rho_{\min}}^{\rho_{\max}} \varphi_{M,\text{scal}}(\rho)\xi_0(\rho)d\rho \quad (15b)$$

$$\begin{aligned} \mathbf{N}_{\text{vect}} &= \hat{\mathbf{x}} \int_{\rho_{\min}}^{\rho_{\max}} \varphi_{N,\text{vect}}(\rho)\xi_c(\rho)d\rho \\ &\quad + \hat{\mathbf{y}} \int_{\rho_{\min}}^{\rho_{\max}} \varphi_{N,\text{vect}}(\rho)\xi_s(\rho)d\rho \quad (15c) \end{aligned}$$

$$N_{\text{scal}} = \int_{\rho_{\min}}^{\rho_{\max}} \varphi_{N,\text{scal}}(\rho)\xi_0(\rho)d\rho. \quad (15d)$$

It is important to note that the kernels $\varphi_{N,\text{vect}}(\rho)$, $\varphi_{N,\text{scal}}(\rho)$ of the integrals in (15c) and (15d) are singular for $\rho \rightarrow 0$, $d = 0$ in evaluating the self-term. However, for such case in (6c), \mathbf{R}^i , \mathbf{N}_{vect} , and ρ^c , lie in the plane of the source triangle. Hence, $\nabla \times \mathbf{\Pi}(\mathbf{r})$ in (6c) is perpendicular to the plane of the source triangle, which is also the observation triangle for the self-term evaluation. Thus when tested with a testing function tangential to the observation triangle (e.g., Galerkin testing, etc.), the resulting contribution always vanishes. Hence, special treatment to take care of the nonremovable singularity in the integrals in (15c) and (15d) is not required for the special case of planar discretization discussed in the paper.

VI. NUMERICAL RESULTS

In this section, the proposed integration schemes are used to compute integrals for all the cases in (15). Comparisons with 2-D Gaussian quadrature are presented along with the results obtained by incorporating the presented technique in a two-region circuit coupled field solver.

For purposes of illustration, and without loss of generality, the source triangle T^{source} for the presented results has nodes

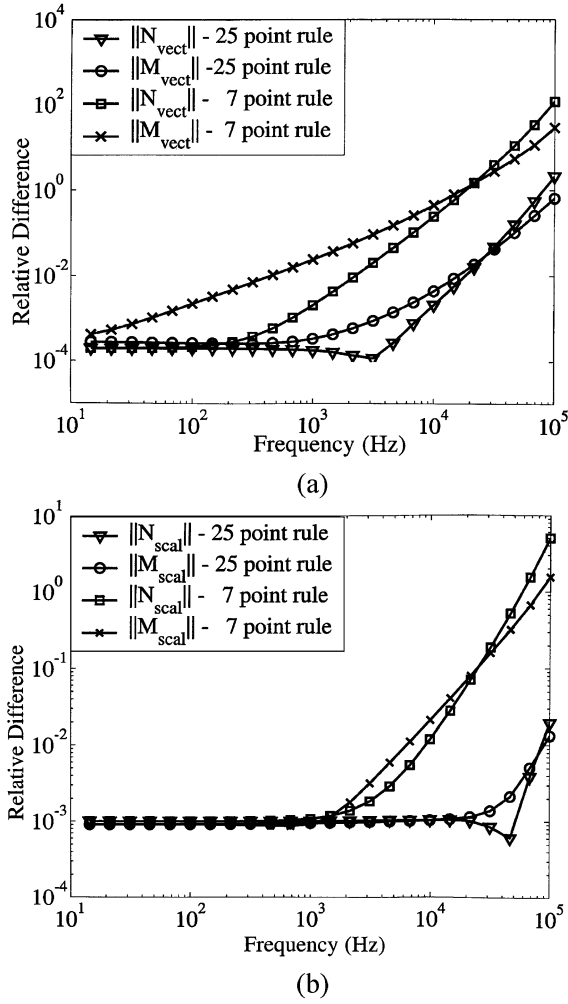


Fig. 2. (a) Comparison between 2-D Gaussian rules with singularity extraction and proposed method for evaluation of the integral N_{vect} , M_{vect} in (7c) and (7a) and (b) N_{scal} and M_{scal} in (7d), (7b) for the non-self-term integral, for a triangle with vertices $(\alpha, -\alpha, 0)$, $(\alpha, \alpha/2, 0)$, $(-2\alpha, \alpha/2, 0)$, and observation point located at $(0, 0, \alpha)$, where $\alpha = 1$ mm, with $\sigma = 5.8 \times 10^7 \text{ Sm}^{-1}$.

located at $(1, -1, 0)$, $(1, 0.5, 0)$, $(-2, 0.5, 0)$, and the observation point P^{obs} lies outside the plane of T^{source} , at $(0, 0, 1)$, with all distances measured in mm. The conductivity of the medium is that of copper $5.8 \times 10^7 \text{ Sm}^{-1}$.

A relative accuracy comparison between the proposed scheme and fixed order 2-D Gaussian quadrature with singularity extraction is demonstrated in Figs. 2 and 3. At low frequencies, the Green's functions in lossy media exhibit slow decay over distance and hence, for example, a seven-point 2-D Gaussian quadrature scheme [13] works adequately, and the relative difference between the two methods is small. As the frequency is increased, the details of the decay in the Green's functions due to the increased imaginary part of the wave-number (2.4) are not captured by the low-order 2-D Gaussian rule and the proposed methodology of this paper is required. The fact that the discrepancy between the results from the proposed method and from low-order 2-D Gaussian quadrature is due to the Gaussian quadrature becoming inaccurate is further evident from comparisons with a higher order 2-D Gaussian quadrature rule using 25 points on a triangle. In

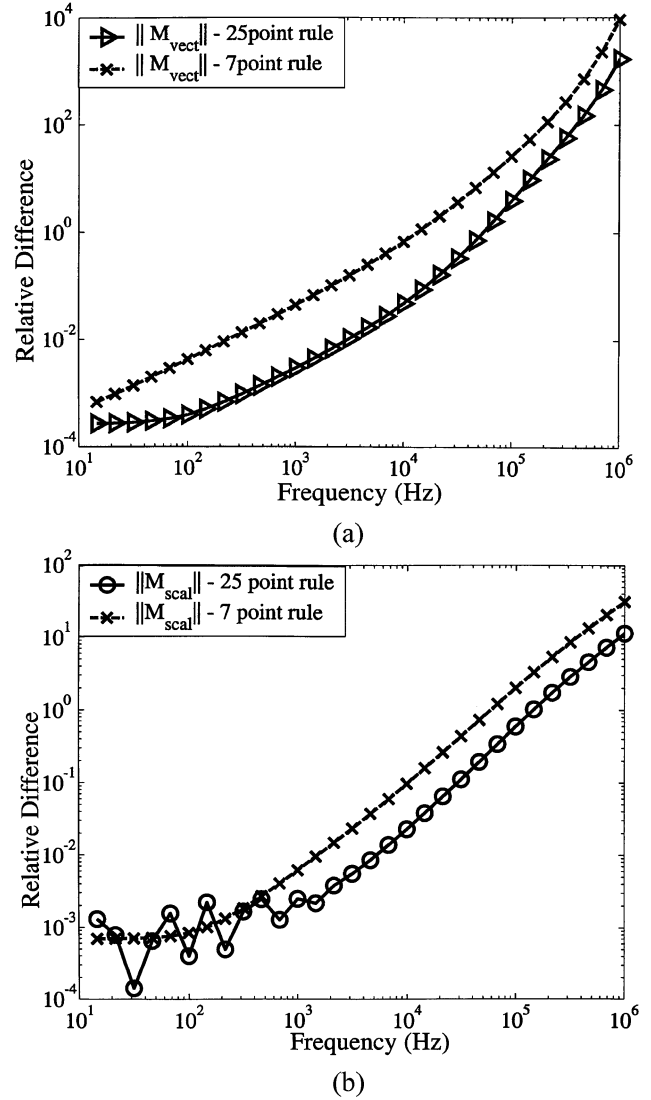


Fig. 3. (a) Comparison between 2-D Gaussian rules with singularity extraction and proposed method for evaluation of the integral M_{vect} in (7a) and (b) M_{scal} in (7b) for the self-term integral, for a triangle with vertices $(\alpha, -\alpha, 0)$, $(\alpha, \alpha/2, 0)$, $(-2\alpha, \alpha/2, 0)$, and observation point located at $(0, 0, 0)$, where $\alpha = 1$ mm, with $\sigma = 5.8 \times 10^7 \text{ Sm}^{-1}$.

this case the frequency at which the 25-point quadrature breaks down increases compared to the seven-point quadrature. In general, for any order of 2-D Gaussian quadrature, there is a frequency point beyond which the fixed order 2-D quadrature will be inaccurate due to insufficient sampling of the details in the decay of the Green's function. The presented method accurately models the decay through an analytic integration and is therefore accurate at any frequency. This is seen in both the vector integrals (15a) and (15c) [Fig. 2(a)] and the scalar integrals (15b) and (15d) [Fig. 2(b)] where the observation point does not lie on the plane of the source triangle. Similar plots for vector (15a) [Fig. 3(a)] and scalar (15b) [Fig. 3(b)] are provided for the self-term integration. While the main aim of this work is the formulation and development of the quadrature rules themselves, one example of the behavior of the rules when included in a complete two-region PMCHW formulation is shown next.

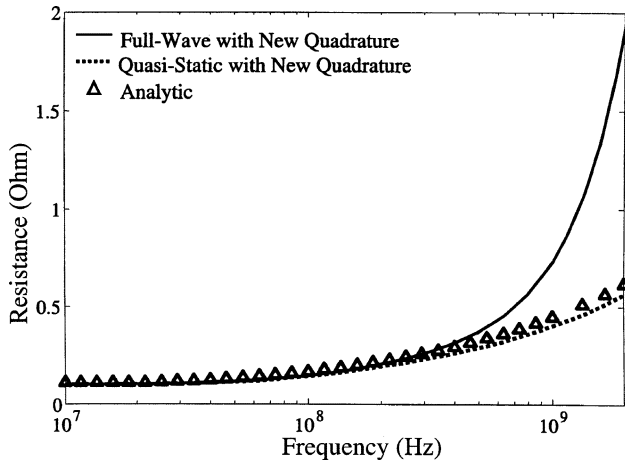
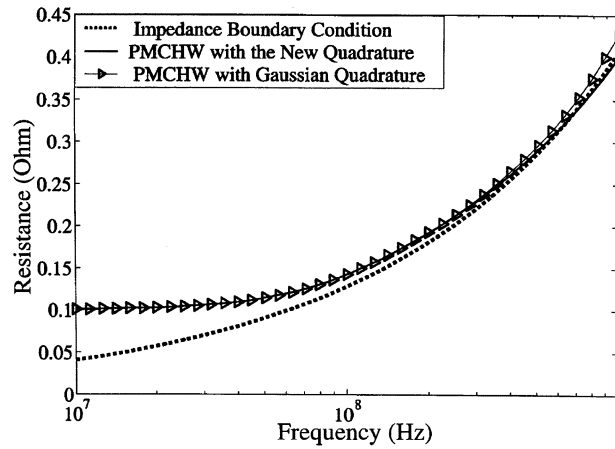
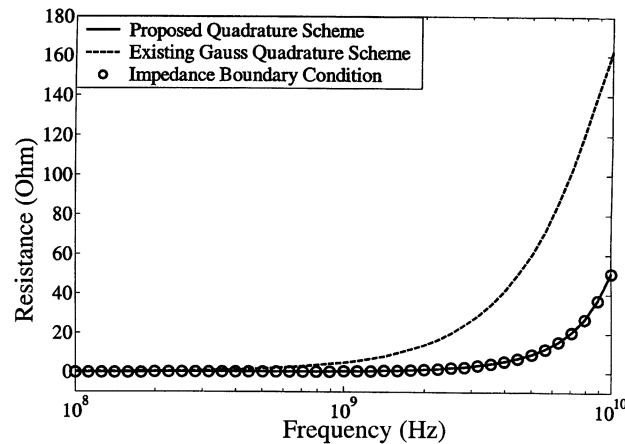


Fig. 4. Extracted resistance of a cylinder with radius 0.5 mm and length 5 mm, using PMCHW formulation with the proposed quadrature scheme, for a full-wave and a quasistatic formulation, and the analytic value of resistance using skin effect approximation.



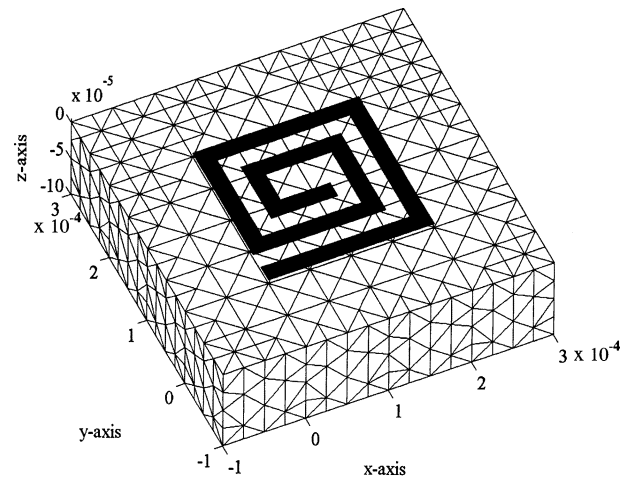
(a)



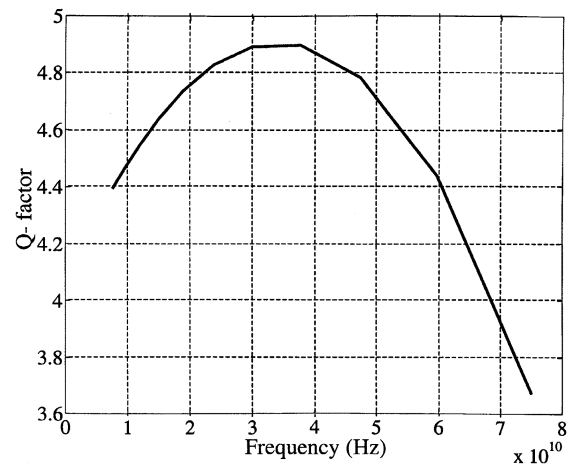
(b)

Fig. 5. Extracted resistance of a cylinder with radius 0.5 mm and length 5 mm, using PMCHW formulation with the proposed quadrature scheme, Gaussian quadrature, and impedance boundary condition for (a) low frequencies and (b) high frequencies .

Fig. 4 demonstrates the comparison between analytic and extracted resistances using the presented quadrature in both quasi-static and full-wave codes.



(a)



(b)

Fig. 6. Q-factor: (a) dimensions and (b) computation of a spiral copper inductor on a substrate with dimensions. Conductivity of the substrate is $1 \times 10^{-5} \text{ Sm}^{-1}$.

As expected, the two codes give same results as analytic computations at low frequencies; eventually, at high frequencies, the full-wave code also predicts additional radiation resistance.

Fig. 5(a) compares the extracted resistance using a coupled circuit-EM formulation [3] and the quadrature scheme presented in this paper, versus standard 2-D Gaussian quadrature rules in the same formulation, as well as versus an (approximate) impedance boundary formulation where interior quadrature is not required [19]. At low frequency, the expected match between the two quadrature-rules is validated (owing to small decay in the Green's function). At high frequencies, [Fig. 5(b)] the new quadrature also matches with the impedance boundary formulation [19] results; the impedance boundary condition is inaccurate at low frequencies [Fig. 5(a)] relative to skin depth, and fails to capture the leveling off of the resistance at low frequency. Conversely, the 2-D Gauss quadrature scheme becomes inaccurate at high frequencies, which is demonstrated in Fig. 5(b). At such frequencies the proposed quadrature scheme produces same result as the impedance boundary condition formulation, while at low frequencies the two quadrature schemes produce the same result. The proposed quadrature scheme has been used to find the Q-factor of a realistic on-chip spiral inductor in Fig. 6.

VII. CONCLUSION

In this paper, a new approach to evaluate the Green's function operators for RWG functions in conducting media is presented. The method works for arbitrarily located sources and observers for any frequency. This technique has been incorporated into a broadband two-region surface formulation for accurate computation of frequency-dependent parameters, and shows the potential to obviate the need to switch to volumetric formulations at frequencies where volumetric current flow is dominant.

ACKNOWLEDGMENT

The authors would like to thank the anonymous reviewers for their comments. The authors also thank D. Gope, Y. Wang, and T. West for their help with numerical simulations.

REFERENCES

- [1] H. Heeb and A. E. Ruehli, "Three-dimensional interconnect analysis using partial element equivalent circuits," *IEEE Trans. Circuits Syst. I*, vol. 39, no. 11, pp. 974–982, Nov. 1992.
- [2] A. Rong and A. C. Cangellaris, "Generalized PEEC models for three-dimensional interconnect structures and integrated passives of arbitrary shapes," in *Proc. Electrical Performance of Electronic Packaging*, Oct. 2001, pp. 225–228.
- [3] V. Jandhyala, W. Yong, D. Gope, and R. Shi, "Coupled electromagnetic-circuit simulation of arbitrarily-shaped conducting structures using triangular meshes," in *Proc. Int. Symp. Quality Electronic Design*, Mar. 2002, pp. 38–42.
- [4] S. Ponnappalli, A. Deutsch, and R. Bertin, "A package analysis tool based on a method of moments surface formulation," *IEEE Trans. Components, Hybrids, Manufact. Technol.*, vol. 16, no. 8, pp. 884–892, Dec. 1993.
- [5] J. Wang, J. Tausch, and J. White, "A wide frequency range surface integral formulation for 3-D RLC extraction," in *Dig. Technical Papers Int. Conf. Computer-Aided Design*, Nov. 1999, pp. 453–457.
- [6] J. Wang, "A New Surface integral formulation of EMQS impedance extraction for 3-D structures," Ph.D. dissertation, Dept. EECS MIT, Cambridge, MA, 1999.
- [7] S. M. Rao, D. R. Wilton, and A. W. Glisson, "Electromagnetic scattering by surfaces of arbitrary shape," *IEEE Trans. Antennas Propagat.*, vol. 30, no. 3, pp. 409–418, May 1982.
- [8] J. S. Zhao and W. C. Chew, "Accurate and efficient simulation of crosstalks," in *Proc. Progress in Electromagnetics Research Symp.*, Boston, MA, July 2002, p. 396.
- [9] S. Chen, J. S. Zhao, and W. C. Chew, "Analyzing low-frequency electromagnetic scattering from a composite object," *IEEE Trans. Geosci. Remote Sensing*, vol. 40, no. 2, pp. 426–433, Feb. 2002.
- [10] K. Umashankar, A. Taflove, and S. M. Rao, "Electromagnetic scattering by arbitrary shaped three dimensional homogeneous lossy dielectric objects," *IEEE Trans. Antennas Propagat.*, vol. 34, no. 6, pp. 758–766, June 1986.
- [11] R. D. Graglia, "On the numerical integration of the linear shape function times the 3-D Green's function or its gradient on a planar triangle," *IEEE Trans. Antennas Propagat.*, vol. 41, no. 10, pp. 1448–1455, Oct. 1993.
- [12] D. R. Wilton, S. M. Rao, A. W. Glisson, D. H. Schaubert, O. M. Al-Bundak, and C. M. Butler, "Potential integrals for uniform and linear source distributions on polygonal and polyhedral domain," *IEEE Trans. Antennas Propagat.*, vol. 32, pp. 276–281, Mar. 1984.
- [13] M. Abramowitz and I. Stegun, *Handbook of Mathematical Functions*. New York: Dover, 1970, ch. 25, pp. 887–894.
- [14] R. E. Hodges and Y. R. Samii, "The evaluation of MFIE integrals with the use of vector triangle basis function," *Microwave Opt. Technol. Lett.*, vol. 14, no. 1, pp. 9–14, Jan. 1997.
- [15] M. Gimersky, S. Amari, and J. Bornemann, "Numerical evaluation of the two-dimensional generalized exponential integral," *IEEE Trans. Antennas Propagat.*, vol. 44, pp. 1422–1425, 1996.
- [16] J. K. Gamage, "Efficient method of moments for compact large planar scatterers in homogeneous medium," in *Proc. 11th Int. Conf. Antennas and Propagation*, Apr. 2001, pp. 741–744.
- [17] Z. Zhu, J. Huang, B. Song, and J. White, "Improving the robustness of a surface integral formulation for wideband impedance extraction of 3-D structures," in *Proc. Int. Conf. Computer Aided Design*, Nov. 2001, pp. 592–597.
- [18] L. Rossi and P. J. Cullen, "On the fully numerical evaluation of the linear-shape function times the 3-D Green's function on a planar triangle," *IEEE Trans. Microwave Theory Tech.*, vol. 47, pp. 398–402, Apr. 1999.
- [19] A. W. Glisson, "Electromagnetic scattering by arbitrarily shaped surfaces with impedance boundary conditions," *Radio Sci.*, vol. 27, no. 6, pp. 935–943, Nov. 1992.



Swagato Chakraborty (S'03) was born in Kolkata, India, on October 3, 1978. He received the B.Tech degree in electronics and electrical communication engineering from the Indian Institute of Technology, Kharagpur, India, in 2001. He is currently working toward the Ph.D. degree in the Applied Computational Electromagnetics (ACE) Group, University of Washington, Seattle.

His research interests include frequency domain integral equation, material models, fast algorithms, coupled circuit-electromagnetic formulations.



Vikram Jandhyala (M'00–SM'03) received the B. Tech degree in electrical engineering from the Indian Institute of Technology, Delhi, in 1993, and the M.S. and Ph.D. degrees from the University of Illinois at Urbana-Champaign, in 1995 and 1998, respectively.

As part of his graduate work, he co-developed the steepest-descent fast-multipole method for rapid simulation of a large class of electromagnetic problems. From 1998 to 2000, he was a Research and Development Engineer at Ansoft Corporation, Pittsburgh, PA. He was involved in the acceleration of Ansoft's

integral equation solvers, and co-developed a fast multipole based extraction tool in Ansoft's Spicelink versions released in 1999 and 2000. Since 2000, he has been an Assistant Professor in the Department of Electrical Engineering, University of Washington, Seattle, where he directs the Applied Computational Electromagnetics Laboratory. He has Visiting Research Status at the Lawrence Livermore National Laboratory, Livermore, CA. He has published more than 70 journal and conference articles. His research interests and projects include several areas of computational electromagnetics, such as fast solvers and integral equation formulations in frequency and time domains, high-speed circuits and devices, coupled multiphysics simulation, novel materials, and propagation.

Dr. Jandhyala is a Full Elected Member of the International Scientific Radio Union (URSI) Commission B. He received an IEEE Microwave Graduate Fellowship for 1996–97, an Outstanding Graduate Research Award from the University of Illinois at Urbana-Champaign, in 1998, and was a recipient of an NSF CAREER Grant in 2001. He has served as a Reviewer for several IEEE journals and conferences and national and international proposal panels, and is on the Technical Program Committee of the IEEE Design Automation Conference and the IEEE Antennas and Propagation Symposium.